

Existence of higher nodal band states with $\alpha+^{48}\text{Ca}$ cluster structure in ^{52}Ti

S. Ohkubo¹

¹*Research Center for Nuclear Physics, Osaka University, Ibaraki, Osaka 567-0047, Japan*
(Dated: April 6, 2020)

It is shown that recently observed α cluster states a few MeV above the α threshold energy in ^{52}Ti correspond to the higher nodal band states with the $\alpha+^{48}\text{Ca}$ cluster structure, i.e. a vibrational mode in which the intercluster relative motion is excited. The existence of the higher nodal states in the ^{48}Ca core region in addition to the well-known higher nodal states in ^{20}Ne and ^{44}Ti reinforces the importance of the concept of vibrational motion due to clustering even in medium-weight nuclei with a jj -shell closed core. The higher nodal band and the shell-like ground band in ^{52}Ti are described in a unified way by a Luneburg lens-like deep local potential due to the Pauli principle, which explains the emergence of backward angle anomaly (anomalous large angle scattering (ALAS)) at low energies, prerainbows at intermediate energies and nuclear rainbows at high energies in $\alpha+^{48}\text{Ca}$ scattering. The existence of a $K = 0^-$ α cluster band analog to ^{44}Ti midway between the ground band and the higher nodal band is inevitably predicted.

The α clustering is essential in the $0p$ -shell and sd shell region and the nuclear structure has been comprehensively understood from the α cluster viewpoint [1]. In the fp shell region, identification of the higher nodal band states with the $\alpha+^{40}\text{Ca}$ cluster structure in the fusion excitation functions [2] lead to the prediction of a $K = 0^-$ band, which is a parity-doublet partner of the ground band, in the typical nucleus ^{44}Ti [3–5]. The observation of the $K = 0^-$ band in experiment [6, 7] showed that the α cluster picture is also essential in ^{44}Ti . Systematic theoretical and experimental studies in the ^{44}Ti region [8–13] confirmed the existence of the α cluster in the beginning of the fp -shell above the double magic nucleus ^{40}Ca .

α clustering aspects in nuclei beyond ^{44}Ti have been explored in the medium weight mass region around $A=50$ such as ^{48}Cr [14, 15] and $^{46,50}\text{Cr}$ [16, 17] as well as in the heavy mass region such as ^{94}Mo and ^{212}Po [18–21]. ^{52}Ti , which is a typical nucleus with two protons and two neutrons outside the doubly closed core ^{48}Ca analog to ^{20}Ne and ^{44}Ti , has been mostly studied in the shell model [22–27]. The ground band 0^+ , 2^+ and 4^+ states are selectively enhanced in the α -transfer reactions such as $^{48}\text{Ca}(^{16}\text{O}, ^{12}\text{C})^{52}\text{Ti}$ [28] and $^{48}\text{Ca}(^{12}\text{C}, ^8\text{Be})^{52}\text{Ti}$ [29]. However a microscopic $\alpha+^{48}\text{Ca}$ cluster model calculation with Brink-Boeker force B1 using the generator coordinate method (GCM) [30] did not give the ground band as well as in the $\alpha+^{40}\text{Ca}$ cluster model calculation for ^{44}Ti . On the other hand, Ohkubo *et al.* [31] and Ohkubo and Hiraoka[32] reproduced the ground band of ^{52}Ti in the α cluster model with a local potential similar to ^{44}Ti [3, 4]. No experimental data that suggest clear α cluster states hampered to conclude that the α cluster picture persists in ^{52}Ti in the jj -shell closed ^{48}Ca core region.

Very recently Bailey *et al.* [33] reported that they newly observed α cluster states at the highly excited energy region in ^{52}Ti . This prompts us to clarify the nature of the observed α cluster states theoretically, especially to which band they belong. In this respect I note that the emergence of a cluster structure is a consequence of the Pauli principle[34], which causes a Luneburg lens-

like deep intercluster potential that accommodates the Pauli-allowed cluster states in the low energy region and a nuclear rainbow due to astigmatism of the lens with a diffuse surface at high energies[34, 35]. The cluster structure and the nuclear rainbow are the two aspects of the phenomena caused by the same Luneburg lens-like inter-nucleus interaction [34]. Therefore it seems useful to clarify the nature of the observed α cluster states in ^{52}Ti from the viewpoint of understanding the ground band states and scattering phenomena for $\alpha+^{48}\text{Ca}$ including nuclear rainbows in a unified way.

The purpose of this paper is to show that the newly observed three α cluster states correspond to the higher nodal states with the $\alpha+^{48}\text{Ca}$ cluster structure in ^{52}Ti by studying the nuclear rainbows at high energies, the Airy structure of the prerainbows at intermediate energies, the backward angle anomaly (anomalous large angles scattering (ALAS)) at low energies, the α cluster structure near the α threshold energy, and the ground state band simultaneously. The existence of a higher nodal excitation mode inevitably predicts the existence of a $K = 0^-$ band state with the α cluster structure midway between the higher nodal band and the ground band in ^{52}Ti .

The anomalous rise of cross sections at backward angles in α particle scattering, ALAS, which was first typically found in α particle scattering from ^{40}Ca [36, 37], is seen persistently in the scattering from the closed nucleus ^{48}Ca [38] at low energies, $E_L=18\text{-}29$ MeV. Stock *et al.* [39] extended the measurement at backward angles to intermediate energies at $E_L=40.7\text{-}65.6$ MeV where prerainbows appear. The nuclear rainbow was observed at high energies above $E_L=100$ MeV [40, 41]. I use a Woods-Saxon squared local potential, which can simulate a Luneburg lens well as in the case of the α cluster study in ^{44}Ti [3, 4]. In the optical model analysis imaginary potentials with a Woods-Saxon and its derivative form factors are introduced, $U(r) = -Vf^2(r; R_v, a_v) + V_{coul}(r) - iWf(r; R_w, a_w) - i4a_s W_s \frac{d}{dr} f(r, R_s, a_s)$ with $f(r; R, a) = 1/\{1 + \exp[(r - R)/a]\}$. The Coulomb potential is assumed to be a uniformly charged sphere with a reduced radius $r_c=1.3$ fm.

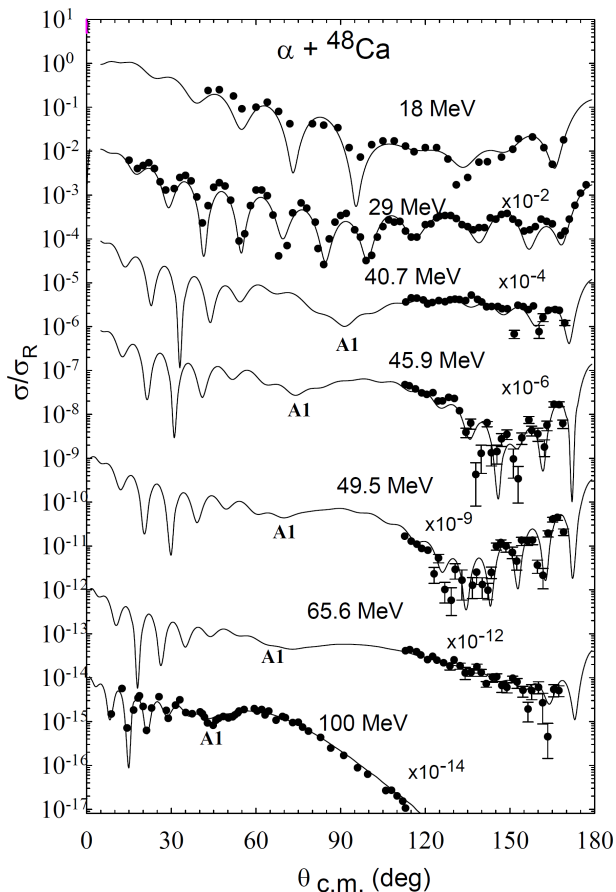


FIG. 1. The angular distributions of cross sections (ratio to Rutherford scattering) in α particle scattering from ^{48}Ca calculated with the optical model potentials in Table I (solid lines) are compared with the experimental data (points) taken from Refs.[38–40]. A1 indicates the Airy minimum.

First I analyze the experimental angular distributions in $\alpha+^{48}\text{Ca}$ scattering with the optical potential model. For the real part of the optical potential, I started from the unique potential used in the systematic analysis of $\alpha+^{40}\text{Ca}$ scattering over a wide range of incident energies [42] and the α cluster structure study of ^{44}Ti [3, 4]. The obtained potential parameters that fit the experimental angular distributions are listed in Table I. At the lower energies below $E_L=29$ MeV the characteristic behavior of ALAS angular distributions rising toward the extreme backward angles, which is difficult to reproduce using the average optical potential as noted in Ref.[38], is slightly seen. The imaginary potential parameters are searched to fit the data. Different from $\alpha+^{40,44}\text{Ca}$ [42], a surface absorption was needed to reproduce the angular distributions at lower energies, which seems to be due to the effect of the extra neutrons in the surface region of ^{48}Ca . Above $E_L=40$ MeV no surface absorption was needed in the analysis. For the real potential the radius parameter r_v is adjusted around 1.35 fm with a fixed $a_v=1.29$. For the imaginary potential r_w and a_w are fixed at 1.25

TABLE I. The optical potential parameters used in Fig. 1 and the volume integrals per nucleon pair, J_v , in unit of MeVfm^3 for the real potentials. E_L , V , W and W_s are in units of MeV and r_v , a_v , r_w , a_w , r_s and a_s are in units of fm.

E_L	J_v	V	r_v	a_v	W	r_w	a_w	W_s	r_s	a_s
18	380	192.6	1.38	1.29	28.1	1.00	0.047	6.3	1.31	0.265
29	342	189	1.34	1.25	28.3	1.02	0.975	4.9	1.41	0.227
40.7	355	180	1.38	1.29	23	1.25	1.0			
45.9	348	180	1.37	1.29	24	1.25	1.0			
49.5	355	180	1.38	1.29	26	1.25	1.0			
65.6	296	160	1.35	1.29	29	1.25	1.0			
100	292	164	1.33	1.29	28.5	1.31	1.0			

and 1.00 fm, respectively, except slight modifications of r_w at $E_L=100$ MeV. In Fig. 1 the calculated results are compared with the experimental data. The calculations reproduce the characteristic feature of the experimental angular distributions well up to the backward angles. Although the experimental data are not available in the forward and intermediate angle regions at $E_L=40.7$ -65.6 MeV, the data at 110 - 140° , which determine the slope of the fall-off in the angular distributions of the prerainbows, are sensitive enough to constraint the real part of the potential. The calculations reproduce the slope of the prerainbows and the characteristic oscillations of the experimental angular distributions. At $E_L=100$ MeV the nuclear rainbow scattering with the lit side minimum at around $\theta=42^\circ$ is reproduced well. The minimum, beyond which the fall-off of the angular distribution in the darkside of the rainbow follows, corresponds to the first Airy minimum A1, which is clearly seen in the angular distribution calculated by switching off the imaginary potential. As seen in Fig. 1, this A1 evolves from the Airy minimum A1 at around 90° at $E_L=40.9$ MeV. The evolution is similar to $\alpha+^{40}\text{Ca}$ scattering in Ref[42].

The appearance of the nuclear rainbow and the Airy structure in the prerainbows, which are sensitive to the internal region of the real part of the potential, shows that the scattering is not strongly absorptive. In the lower energies at 29 and 18 MeV where the ALAS appears as a precursor of the prerainbows, scattering is also sensitive to the internal region of the potential. In Fig. 2 the calculated angular distributions at $E_L=18$ and 29 MeV are decomposed using the technique of Ref.[43] into the barrier-wave component reflected at the surface and the internal-wave component, which penetrates deep into the internal region of the potential, are displayed. In the last peak of the angular distribution toward 180° , the internal-wave contribution is dominated. However, the interference of the two components, which is seen only in the intermediate angles in the $\alpha+^{40}\text{Ca}$ system, occurs even at the backward angles. The characteristic behavior of the experimental angular distribution beyond $\theta=90^\circ$ is well reproduced by the interference between the internal-wave and the barrier-wave contributions. In the

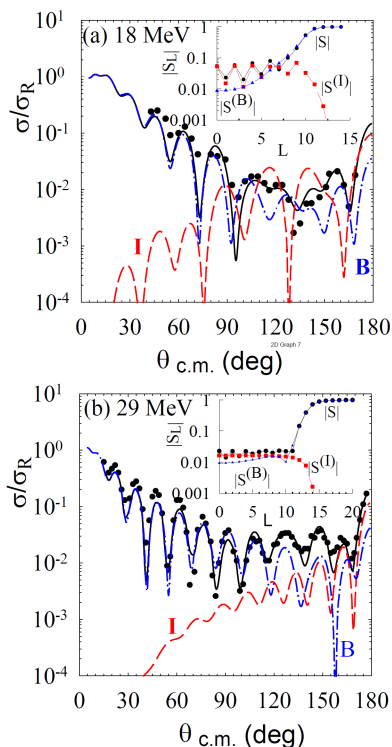


FIG. 2. (Color online) The calculated angular distributions of cross sections (ratio to Rutherford scattering) in α particle scattering from ^{48}Ca (solid lines) at (a) $E_L=18$ and (b) 29 MeV in Fig. 1 are decomposed into the internal-wave (dashed lines) and the barrier-wave (dash-dotted lines) contributions. The points are the experimental data from Ref.[38]. In the insets, the reflection coefficient ($|S_L|$) is decomposed into the internal-wave ($|S_L^{(I)}|$) and the barrier-wave ($|S_L^{(B)}|$). The lines are to guide the eye.

insets, one sees that at 18 MeV the reflection coefficient of the internal-wave is considerably larger than that of the barrier-wave for the low partial waves, which shows that scattering is transparent.

The real part of the optical potential obtained in the analysis of α particle scattering is useful for the α -cluster structure study in ^{52}Ti . The strength of the real part of the optical potentials is known to have energy dependence to decrease toward the threshold (threshold anomaly) [44] and the strength must be adjusted in the α cluster calculations. In fact, the lowest Pauli-allowed state obtained using the potential at $E_L=18$ MeV (29 MeV) is overbinding compared with the experimental value of -7.76 MeV. In Fig 3 the energy levels calculated in the bound state approximation using the potential at 18 MeV in Table I with the adjusted strength $V=166.8$ MeV, which is tuned to reproduce the binding energy of the ground state, are shown. The states with $N = 2n+L < 12$ and $L = 12$ with $N = 12$ are forbidden by the Pauli principle where n and L are the number of nodes in the wave functions and the orbital angular momentum of the relative motion, respectively. The cal-

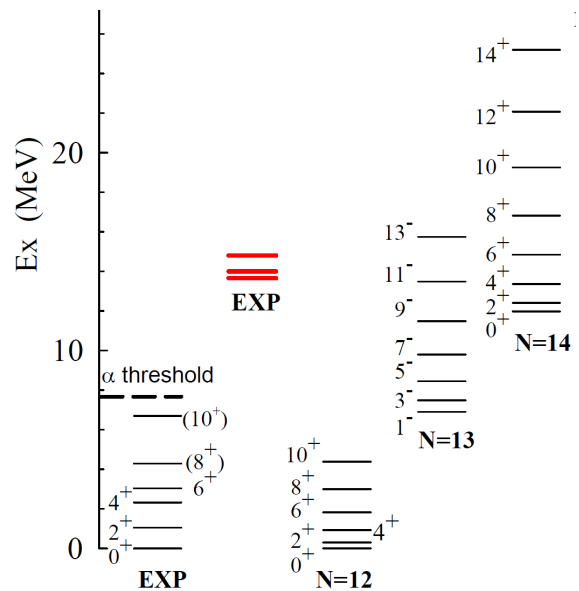


FIG. 3. Calculated energy levels of ^{52}Ti are compared with the experimental ground band [45] and the newly observed three excited α cluster states (red thick solid lines) [33].

culated $J_\nu=329$ MeVfm³ of the potential is comparable to 350 MeVfm³ for the $\alpha+^{40}\text{Ca}$ system [4]. The calculated ground band states fall well in correspondence to the experimental ground band. The observed higher spin states show antistretching deviating from a rotational-like spectrum similar to ^{20}Ne [46] and ^{44}Ti , which can be reproduced by taking into account the L -dependence of the potential, as discussed in the α cluster structure in ^{20}Ne [46], ^{44}Ti [3, 4], ^{94}Mo [18, 47], ^{212}Po [18, 48] and recently in $^{46,50}\text{Cr}$ [17].

In Table II one sees that the calculated $B(E2)$ values of the ground band are considerably large compared with the single particle unit $11.5 e^2\text{fm}^4$ and in agreement with the observed values without effective charges. In the shell model calculations in the fp-shell nuclei, usually large effective charges, such as $e_\pi=1.3-1.5$ and $e_\nu=0.6-0.8$ in Ref.[24] are needed to reproduce the experimental $B(E2)$ values. The large $B(E2)$ values come from the collectivity due to the α -clustering and one of the origins of the large effective charge may be ascribed to the α -clustering degree of freedom. The rms distance between the α particle and the ^{48}Ca core of the ground band is considerably smaller than 5.15 fm, the sum of the rms charge radii of the free α (1.676 fm) and ^{48}Ca (3.477 fm) [50]. The two clusters overlap significantly.

In Fig. 3 the calculation predicts the $N = 14$ α cluster band above the α threshold energy. One sees that the newly observed three α cluster states in Ref.[33] correspond in excitation energy to the 0^+ , 2^+ and 4^+ states of the $N = 14$ band. The energy intervals among the three states also correspond to the calculation well. In fact, the ratio $R = (E_x(4^+) - E_x(0^+))/(E_x(2^+) - E_x(0^+)) \simeq 3.4$ for the observed three states, which shows that they can

TABLE II. (Color online) The calculated energy with respect to the α threshold E , excitation energy E_x , intercluster rms radii $\langle R^2 \rangle^{1/2}$ and $B(E2)$ values in unit of $e^2\text{fm}^4$ for the $J \rightarrow J - 2$ transitions for the $N = 12$ and $N = 13$ band states in ^{52}Ti . Theoretical $B(E2)$ values are compared with the experimental data [49] and the shell model calculations [24].

J	$N = 12$						$N = 13$				
	E (MeV)	E_x (MeV)	$\langle R^2 \rangle^{1/2}$ (fm)	$B(E2) (J \rightarrow J - 2)$			E (MeV)	E_x (MeV)	$\langle R^2 \rangle^{1/2}$ (fm)	$B(E2) (J \rightarrow J - 2)$	
				exp.[49]	This work	Ref.[24]				This work	
0^+	-7.66	0.0	4.57				1^-	-0.76	6.90	5.05	
2^+	-7.36	0.31	4.53	86_{-4}^{+5}	108	100	3^-	-0.18	7.48	4.99	212
4^+	-6.73	0.93	4.50	109_{-13}^{+16}	142	134	5^-	0.79	8.45	4.89	223
6^+	-5.83	1.83	4.39	100_{-6}^{+7}	134	88.6	7^-	2.14	9.80	4.74	196
8^+	-4.67	2.99	4.28	8.8_{-1}^{+1}	109		9^-	3.82	11.48	4.56	152
10^+	-3.27	4.39	4.16		76		11^-	5.82	13.48	4.37	100

TABLE III. Resonance energies and widths for the $N = 14$ band states in ^{52}Ti , together with the corresponding dimensionless reduced widths θ^2 calculated with channel radii $a=7.5$ and 8 fm.

J	E_{res} (MeV)	Γ_L (keV)	θ_L^2 (%)	
			$a = 7.5$	$a = 8.0$
0^+	4.66	33	78	46
2^+	5.12	62	100	59
4^+	6.16	60	56	33
6^+	7.77	74	45	25
8^+	9.92	47	22	12
10^+	12.55	29	12	6
12^+	15.60	7	3	1
14^+	18.98	<1	<1	<1

be considered to form a rotational band, agrees well with $R = 3.2$ of the theoretical $N = 14$ band. Also the estimated rotational constant $k \simeq 57$ keV for the observed states is close to the theoretical $k = 69$ keV for the $N = 14$ band where $k \equiv \hbar^2/2\mathcal{J}$ with \mathcal{J} being the moment of inertia. Here it is to be noted that the four states observed in ^{44}Ti [33] using the same technique as in ^{52}Ti also correspond to the 0^+ , 2^+ , 4^+ and 6^+ states of the $N = 14$ band [9, 12] well. The identification of the $N=14$ higher nodal band a few MeV above the α threshold energy as an analog band observed in ^{44}Ti , in which relative motion between α and ^{48}Ca is one more excited compared with the ground band, gives strong support to α clustering in ^{52}Ti . The intercluster rms radii of the $N = 14$ band calculated in the bound state approximation, 5.99, 5.95, 5.84, 5.65 and 5.36 fm for the 0^+ , 2^+ , 4^+ , 6^+ , and 8^+ states, respectively, are larger than the sum of those of the free α and ^{48}Ca nuclei, which shows that this band has a well-developed α cluster structure. The degree of α clustering is more clearly seen in the considerably large dimensionless reduced widths θ_L^2 in Table III, which are calculated from the α decay width Γ_L at the reso-

nance energy E_{res} using the formula $\Gamma_L = 2P_L(a)\gamma_L^2(a)$, $\gamma_L^2(a) = \theta_L^2(a)\gamma_w^2(a)$ and $\gamma_w^2(a) = 3\hbar^2/2\mu a$ with $P_L(a)$, $\gamma_L^2(a)$ and $\gamma_w^2(a)$ being the penetration factor, reduced width and the Wigner limit value at a channel radius a , respectively. μ is the reduced mass. Γ_L is calculated from the phase shift δ_L using $\Gamma_L = 2/(\frac{\partial \delta_L}{\partial E_{c.m.}})_{E_{c.m.}=E_{res}}$.

In Fig. 3 the calculation inevitably locates the $N = 13$ $K = 0^-$ band with the $\alpha+^{48}\text{Ca}$ structure midway between the ground band ($N = 12$) and the higher nodal band ($N = 14$). The $K = 0^-$ band, which starts near the α -threshold, is a parity-doublet partner of the ground band. The existence of such a $N = 13$ $K = 0^-$ band between the ground band and the higher nodal band has been already confirmed experimentally in ^{44}Ti [6, 7, 10, 13]. The calculated intercluster distances of the band states in Table II are slightly smaller than those calculated for the $N = 13$ band in ^{44}Ti [3]. This suggests the α clustering of this band is smaller than that in ^{44}Ti . I confirmed that almost the same band structure as in Fig. 3 is obtained in the calculations using the potential at $E_L=29$ MeV in Table I with the strength V adjusted to reproduce the binding energy of the ground state. The experimental observation of the member states of the $N = 13$ band would give further support to α clustering with the parity-doublet structure in the ^{48}Ca core region.

In Fig. 4 the potential at $E_L=18$ MeV is displayed in comparison with a Luneburg lens [51] potential, which decreases radially from the center to the outer surface $r = R_0$ and refracts all the parallel incident trajectories to the focus $r = R_f$ ($< R_0$). The Luneburg lens potential is a truncated harmonic oscillator potential [35] given by $V(r) = V_0 (r^2/R_0^2 - 1)$ for $r \leq R_0$ and $V(r) = 0$ for $r > R_0$. One sees that in the internal region $r < 5$ fm the potential resembles the Luneburg lens potential. This is the reason why the present potential that embeds the Pauli-forbidden states with $N < 12$ deeply in the potential locates the $N = 12$ and $N = 14$ cluster band states in correspondence to experiment and predicts the unobserved $N = 13$ band. The diffuse surface of the potential at $r > 5$ fm where deviation from the Luneburg

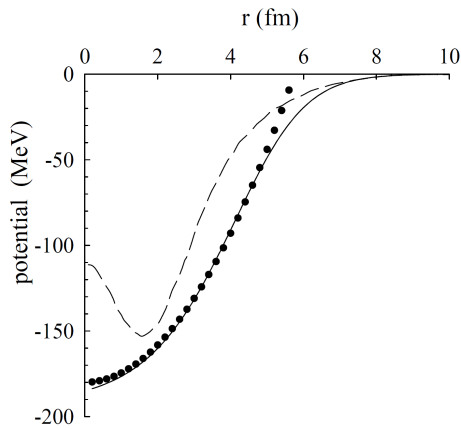


FIG. 4. The α - ^{48}Ca potential at $E_L = 18$ MeV (solid line) is compared with the Luneburg lens potential with $R_0 = 5.75$ fm and $V_0 = 180$ MeV (points). The energy-independent equivalent local potential (for $L = 0$) in the GCM calculation from Ref.[52] is shown by the dashed line.

lens is clear causes astigmatism of the lens, i.e., nuclear rainbow at high energies. The volume integral per pair nucleon pair, $J_v = 342$ MeVfm 3 at 29 MeV, is as large as $J_v = 345$ MeVfm 3 of the potential by Michel and Vanderpoorten [53] obtained in the model-independent analysis of the angular distribution at $E_L = 29$ MeV. The volume integral is also consistent with the value of the global potential for the $\alpha + ^{40}\text{Ca}$ system, 350 MeVfm 3 [53] at the

same energy. One finds that, in Fig. 4, the equivalent local potential [52] of the microscopic GCM cluster model calculation[30] belongs to a shallower potential family, which is unable to describe the nuclear rainbow. This explains why the lowest Pauli-allowed band with $N = 12$ corresponding to the ground band does not appear below the α threshold energy in Ref. [30].

To summarize, the newly observed three α cluster states are found to correspond to the $N = 14$ higher nodal band states, the 0^+ , 2^+ and 4^+ states, which are the nodal excited states of the relative motion of the $\alpha + ^{48}\text{Ca}$ cluster structure in ^{52}Ti . This gives strong support to the persistence of the α cluster structure in ^{52}Ti . The calculated lowest Pauli-allowed $N = 12$ band is found to correspond well to the experimental ground band and the large experimental $B(E2)$ values are reproduced without effective charge. The local potential that describes backward angle anomaly (anomalous large angle scattering), prerainbows and nuclear rainbow in a wide range of incident energies in $\alpha + ^{48}\text{Ca}$ scattering, the $N = 14$ and $N = 12$ α cluster bands, predicts inevitably the existence of a $K = 0^-$ band ($N = 13$), which is a parity-doublet partner of the ground band, near the α threshold midway between the ground band and the $N = 14$ higher nodal band. Observation of the $K = 0^-$ band states would give further support to α clustering in the jj -shell closed ^{48}Ca region.

The author thanks the Yukawa Institute for Theoretical Physics, Kyoto University for hospitality extended during a stay in 2019.

-
- [1] Y. Fujiwara, H. Horiuchi, K. Ikeda, M. Kamimura, K. Kato, Y. Suzuki, and E. Uegaki, *Suppl. Prog. Theor. Phys.* **68**, 29 (1980) and references therein.
- [2] F. Michel, G. Reidemeister, and S. Ohkubo, *Phys. Rev. C* **34**, 1248 (1986).
- [3] F. Michel, G. Reidemeister, and S. Ohkubo, *Phys. Rev. Lett.* **57**, 1215 (1986).
- [4] F. Michel, G. Reidemeister, and S. Ohkubo, *Phys. Rev. C* **37**, 292 (1988).
- [5] S. Ohkubo, *Phys. Rev. C* **38**, 2377 (1988).
- [6] T. Yamaya, S. Oh-ami, M. Fujiwara, T. Itahashi, K. Katori, M. Tosaki, S. Kato, S. Hatori, and S. Ohkubo, *Phys. Rev. C* **42**, 1935 (1990).
- [7] P. Guazzoni, M. Jaskola, L. Zetta, C. Y. Kim, T. Udagawa, and G. Bohlen, *Nucl. Phys.* **A564**, 425 (1993).
- [8] S. Ohkubo, M. Fujiwara, and P. E. Hodgson, *Prog. Theor. Phys. Suppl.* **132**, 1 (1998).
- [9] F. Michel, S. Ohkubo, and G. Reidemeister, *Prog. Theor. Phys. Suppl.* **132**, 7 (1998).
- [10] T. Yamaya, K. Katori, M. Fujiwara, S. Kato, and S. Ohkubo, *Prog. Theor. Phys. Suppl.* **132**, 73 (1998).
- [11] T. Sakuda and S. Ohkubo, *Prog. Theor. Phys. Suppl.* **132**, 103 (1998).
- [12] S. Ohkubo, Y. Hirabayashi, and T. Sakuda, *Phys. Rev. C* **57**, 2760 (1998).
- [13] M. Fukada, M. K. Takimoto, K. Ogino, and S. Ohkubo, *Phys. Rev. C* **80**, 064613 (2009).
- [14] P. Descouvemont, *Nucl. Phys.* **A 709**, 275 (2002).
- [15] T. Sakuda and S. Ohkubo, *Nucl. Phys.* **A 712**, 59 (2002).
- [16] M. A. Souza and H. Miyake, *Eur. Phys. J.* **A 53**, 146 (2017).
- [17] P. Mohr, *Eur. Phys. J.* **A 53**, 209 (2017).
- [18] S. Ohkubo, *Phys. Rev. Lett.* **74**, 2176 (1995).
- [19] B. Buck, A. C. Merchant, and S. M. Perez, *Phys. Rev. C* **51**, 559 (1995).
- [20] F. Michel, G. Reidemeister, and S. Ohkubo, *Phys. Rev. C* **61**, 041601(R) (2000).
- [21] S. Ohkubo, *Int. J. Mod. Phys. A* **14**, 2035 (2009).
- [22] J. B. McGrory, *Phys. Rev.* **160**, 915 (1967).
- [23] H. Horie and K. Ogawa, *Nucl. Phys.* **A216**, 407 (1973).
- [24] H. Nakada, T. Sebe, and T. Otsuka, *Nucl. Phys.* **A571**, 467 (1994).
- [25] S. Zhu, R. V. F. Janssens, B. Fornal, S. J. Freeman, M. Honma, R. Broda *et al.*, *Phys. Rev. C* **80**, 024318 (2009).
- [26] D.-C. Dinca, R. V. F. Janssens, A. Gade, D. Bazin, R. Broda, B. A. Brown *et al.*, *Phys. Rev. C* **71**, 041302(R) (2005).
- [27] R. V. F. Janssens, B. Fornal, P. F. Mantica, B. A. Brown, R. Broda, P. Bhattacharyya *et al.*, *Phys. Lett.* **B 546**, 55 (2002).
- [28] H. Faraggi, M.-C. Lemaire, J. M. Loiseaux, M. C. Mermaz, and A. Papineaux, *Phys. Rev. C* **4**, 1375 (1971); H. Faraggi, *J. de Phys. Collq.* **32**, C6-25 (1971).
- [29] E. Mathiak, K. A. Eberhald, J. G. Cramer, H. H. Ross-

- ner, J. Stettemeier, and A. Weidinger, Nucl. Phys. **A259**, 129 (1976).
- [30] K. Langanke, Nucl. Phys. **A377**, 53 (1982).
- [31] S. Ohkubo, K. Umehara, and K. Hiraoka, *Developments of nuclear cluster dynamics*, edited by Y. Akaishi, K. Kato, H. Noto, and S. Okabe, (World Scientific, 1989), p 114.
- [32] S. Ohkubo and K. Hiraoka, Bull. Kochi Women's Univ. Natural Sci. **40**, 13 (1992).
- [33] S. Bailey, T. Kokalova, M. Freer, C. Wheldon, R. Smith, J. Walshe *et al.*, Phys. Rev. C **100**, 051302(R) (2019).
- [34] S. Ohkubo, Phys. Rev. C **93**, 041303(R) (2016).
- [35] F. Michel, G. Reidemeister, and S. Ohkubo, Phys. Rev. Lett. **89**, 152701 (2002).
- [36] A. Budzanowski, K. Grotowski, L. Jarczyk, B. Lazarka, S. Micik, H. Niewodniczański, A. Strzalkowski, and Mrs. Z. Wróbel, Phys. Lett. **16**, 135 (1965).
- [37] C. R. Gruhn and N. S. Wall, Nucl. Phys. **81**, 161 (1966).
- [38] G. Gaul, H. Ludecke, R. Santo, H. Schmeing, and R. Stock, Nucl. Phys. **A137**, 177 (1969).
- [39] R. Stock, G. Gaul, R. Santo, M. Bernas, B. Harvey, D. Hendrie, J. Mahoney, J. Sherman, J. Steyaert, and M. Zisman, Phys. Rev. C **6**, 1226 (1972).
- [40] H. Eickhoff, D. Frekers, H. Löhner, K. Poppensieker, R. Santo, G. Gaul, C. Mayer-Borricke, and P. Turek, Nucl. Phys. **A252**, 333 (1975).
- [41] H. J. Gils, E. Friedman, H. Rebel, J. Buschmann, S. Zagromski, H. Klewe-Nebenius, B. Neumann, R. Pesl, and G. Bechtold, Phys. Rev C **21**, 1239 (1980).
- [42] Th. Delbar, Gh. Grégoire, G. Paić, R. Ceuleneer, F. Michel, R. Vanderpoorten *et al.*, Phys. Rev. C **18**, 1237 (1978).
- [43] J. Albiński and F. Michel, Phys. Rev. C **25**, 213 (1982).
- [44] C. Mahaux, H. Ngo, and G. R. Satchler, Nucl. Phys. **A449**, 354 (1986); **A456**, 134 (1986).
- [45] Y. Dong and H. Junde, Nucl. Data Sheets **128**, 185 (2015).
- [46] F. Michel, Y. Kondo, and G. Reidemeister, Phys. Lett. **B 220**, 479 (1989).
- [47] M. A. Souza and H. Miyake, Phys. Rev. C **91**, 034320 (2015).
- [48] D. Ni and Z. Ren, Phys. Rev. C **83**, 014310 (2011).
- [49] A. Goldkuhle *et al.*, Phys. Rev. C **100**, 054317 (2019).
- [50] I. Angeli and K. P. Marinova, Atomic Data and Nucl. Data Tables, **99**, 69 (2013).
- [51] R. K. Luneburg, *Mathematical Theory of Optics* (University of California Press, Oakland, California, 1964).
- [52] D. Wintgen, H. Friedrich, and K. Langanke, Nucl. Phys. **A408**, 239 (1983).
- [53] F. Michel and R. Vanderpoorten, Phys. Lett. **82B**, 183 (1979).